THE CONNECTION BETWEEN DEEP EASTERN EQUATORIAL PACIFIC OCEAN OXYGENATION AND ATMOSPHERIC CO_2 OVER THE PAST 180 KYR

A Thesis

by

RYAN MICHAEL HOSTAK

Submitted to the Office of Graduate and Professional Studies of
Texas A&M University
in partial fulfillment of the requirements for the degree of

MASTER OF SCIENCE

Chair of Committee,	Franco Marcantonio
Committee Members,	Christina Belanger
	Brendan Roark
	Yige Zhang
Head of Department,	Michael Pope

May 2019

Major Subject: Geology

ABSTRACT

Ventilation of carbon stored in the deep ocean is thought to play an important role in atmospheric CO_2 increases associated with the Pleistocene deglaciations. The presence of this respired carbon has been recorded by an array of palaeoceanographic proxies in broad swaths of the global ocean, including the Eastern Equatorial Pacific (EEP). Today, the Eastern Equatorial Pacific is a significant source of CO_2 to the atmosphere and accounts for a significant proportion of global export productivity. Here we present a new, 180,000-year sediment core from the EEP and reconstruct ^{230}Th derived fluxes of ^{232}Th and barium, along with redox-sensitive uranium concentrations to examine past variations in Fe-bearing dust delivery, export productivity, and bottom-water oxygenation, respectively. We compare these to similar records from the equator in order to infer changes in local atmospheric circulation and bottom-water oxygenation over the past 95,000 years. We then discuss these EEP uranium records in the context of similar, global records, highlighting the importance of the deep EEP and Southern Ocean in deep-ocean respired carbon storage.

ACKNOWLEDGEMENTS

I would like to thank my committee chair and advisor Dr. Franco Marcantonio, as well as my committee members Dr. Christina Belanger, Dr. Yige Zhang and Dr. Brendan Roark, for their guidance and support through the course of this research. Moreover, I would like to thank Dr. Marcantonio for affording me the opportunity to work in the Ken William's Radiogenic Isotope Geochemistry Lab as an undergrad allowed me to gain important lab skills while cultivating my interest in paleoceanography. I would also like to thank my lab mentors Matthew Loveley and Marilyn Wisler, who consistently and professionally provided me with the necessary knowledge and tools to perform quality analytical work. I would like to thank our technical lab coordinator, Luz Romero, for her support through all of the analytical work inherent to this thesis. Thanks also go to the many undergraduate students who I've had the opportunity to work with during this course of research. Camille VanEgmond, John Tye and Erik Urquidi, thank you especially for your time and commitment. Lastly, thank you to my undergraduate and graduate advisors, Suzanne Rosser and Patricia Fike, for guiding me through my time at Texas A&M University.

CONTRIBUTORS AND FUNDING SOURCES

This work was supervised by a thesis committee consisting of Professors Marcantonio (advisor) and Belanger of the Department of Geology and Geophysics and Professors Yhang and Roark of the Department of Oceanography. Ryan Hostak sampled core MV1014-8JC and performed the U-Th-Ba analyses with the help of Matthew Loveley, Marilyn Wisler, Camille VanEgmond, John Tye and Erik Urquidi with technical assistance from Luz Romero. Matthew Loveley performed the oxygen isotope analysis.

This research was funded by NSF grants 1803803 and 1803933, awarded to Franco Marcantonio and Matthew Schmidt, respectively. Additional financial support was provided by Franco Marcantonio and the Office of Graduate Studies (OGS) through the Lechner Graduate Grant Program.

TABLE OF CONTENTS

Page

LIST OF FIGURES

Page

1. INTRODUCTION

The dominant signal in global climate over the last 800,000 years is the 100-kyr co-varying temperature and carbon dioxide variations observed in the EPICA Antarctica ice core (Bereiter et al., 2012). The temperature variations are likely modulated by the 100-kyr eccentricity signal, and amplified by climate feedbacks which involve atmospheric CO_2. The cause of atmospheric CO_2 variability over late Pleistocene glacial-interglacial cycles is still debated, with a variety of explanations from changes in ocean stratification and ventilation, efficiency of the biological pump and nutrient availability, and carbonate compensation depth (Jaccard et al., 2016; Anderson et al., 2009; Toggweiler, 1999; Lamy et al., 2014; Jaccard et al., 2009; Mekik et al. 2012). One popular hypothesis is that there is an increased storage of respired carbon in the deep ocean during glacial maxima. This respired pool of carbon is isolated from interaction with the atmosphere (Broecker, 1982; Bradtmiller et al., 2010; Anderson et al., 2009). Significant ventilation of this pool of respired carbon is thought to occur in the Southern Ocean and is coincident with upwelling there during the deglaciation, and on millennial timescales during the last glaciation (Jaccard et al., 2016; Anderson et al., 2009).

Like the Southern Ocean, the eastern equatorial Pacific Ocean (EEP) plays an important role in the global carbon cycle. Today, although the EEP is the major source of oceanic CO_2 outgassed to the atmosphere (Takahashi et al., 2009), approximately 5-10% of annual global export production occurs there (Field et al., 1998). Thus, although the EEP is a net CO_2 source to the atmosphere today, it could easily have been a CO_2

sink in the past, for example, if sequestering of CO_2 by the biological pump were more efficient.

Here we present proxy data of bottom water oxygenation (authigenic U, see Methodology), biological productivity (^{230}Th-derived excess Ba (xsBa) flux, see Methodology), and dust (^{230}Th-derived ^{232}Th flux, see Methodology) flux from a high-sedimentation-rate core from the Panama Basin of the EEP (MV1014-8JC, *6° 14.0' N, 86° 02.6' W; 1993 m water depth*). Our record spans the past 180 kyr beginning in the penultimate glacial period (marine oxygen isotope stage, MIS 6) at sub-millennial resolution. Core MV1014-8JC (8JC) was collected on the Cocos Ridge in the Panama Basin. We constructed an age model using (a) radiocarbon measurements of the foraminiferal species, *N. dutertrei*, (b) identification of the Los Chocoyos ash at 311 cm in the core (well dated at 84 kyr; Rose et al., 1999), and (c) tying the 8JC δ^{18}O record (*N. dutertrei*) to the LRO4 global oxygen isotope record (Lisiecki and Raymo, 2004) using the software Analyseries (Paillard et al., 1996). The sedimentation rate at site 8JC varies from 1.3 to 6.8 cm/kyr, giving an age resolution of ~300-900 yrs during MIS 1-4 and ~750-2000 yrs during MIS 5 and 6 for our sampling resolution of 2 cm.

Through these records of dust flux (^{232}Th), biological productivity (xsBa) and bottom water oxygenation (aU), we aim to better understand how reduced Fe limitation via increased dust deposition might have increased export production in the glacial EEP both within (MV1014-17JC; Loveley et al., 2017), and to the north of (8JC), the Pacific cold tongue. Furthermore, we examine the relationship between an export production proxy, xsBa, and a redox-sensitive proxy, aU, in an effort to unravel the relative contributions of organic matter flux and bottom water oxygen concentrations to pore

water redox conditions. We conclude that our two aU records may be reflecting the extent and reach of a deep-ocean respired carbon pool in the EEP and its relationship to variations in atmospheric CO_2 during the past 180 kyr.

2.1. Dust Fluxes in the EEP and ITCZ Significance

Increased pulses of dust during the deglaciation and northern hemisphere Heinrich Stadial (HS) events suggest a link between changes in atmospheric circulation in the EEP and changes in Atlantic Meridional Overturning Circulation (AMOC) (Loveley et al., 2017). An AMOC slowdown (McManus et al., 2004, Kienast et al., 2006) during the deglaciation and the HS1 event is coincident with the shifting of wind belts, specifically the Intertropical Convergence Zone (ITCZ) and the westerlies of both

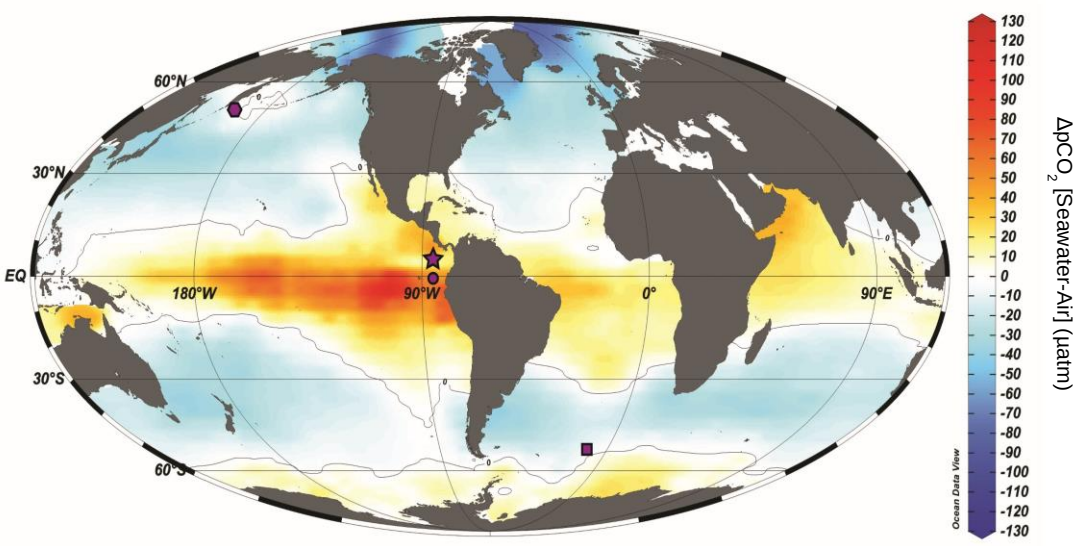

Figure 2-1
Global ΔpCO_2 flux and study core locations. Map created in Ocean Data View using ΔpCO_2 flux data from Takahashi et al. (2009). Core locations for authigenic uranium records compared in this study are denoted on the map as follows: Subarctic North Pacific site ODP 882 (Hexagon), Eastern Equatorial Pacific sites MV1014-8JC (Star) and MV1014-17JC (Circle) and Southern Ocean sites TN057-13/14PC (Square).

hemispheres (Peterson et al., 2000). At site 8JC in the EEP (Figure 2-1, star), there are

significant increases in ^{230}Th-derived ^{232}Th fluxes (dust flux proxy) during deglacial terminations (near the ends of Marine Oxygen Isotope Stages (MIS), 2 and 6) and associated HS events (HS1 and HS11; Figure 2-2 C). Notably, two to three-fold increases in ^{230}Th-derived ^{232}Th fluxes from "baseline" interglacial values of ~1.3 μg cm^{-2} kyr^{-1} at HS1 (~15kya, end MIS 2) and HS11 (~129-136 kya, end MIS 6) indicate a link between periods of deglaciation and increased northern hemisphere dust supplied to the EEP. In addition, beyond the effects of bioturbation of the Los Chocoyos ash, at about 60 kyr towards the end of MIS 4 and near HS6, there is a similar 2-fold increase in ^{230}Th-derived ^{232}Th flux above "ambient" values. The duration of these "peaks" in ^{230}Th-derived ^{232}Th flux (~5 kyr) is of significant value for climate modeling, as they demonstrate and agree with other studies that show that the tropical Pacific records peak glacial conditions and a dustier atmosphere within short pulses at the end of glacial periods (Winckler et al., 2008; Anderson et al., 2006; McGee et al, 2016; Costa et al., 2016; Jacobel et al., 2016; Loveley et al., 2017).

The lack of significant variability in ^{230}Th-derived ^{232}Th flux at site 8JC outside of glacial terminations (i.e., Terminations I and II; HS1 and HS11) and at the end of MIS 4 (HS6) can be compared to the variability observed at the more southern site MV1014-17JC (17JC) (Loveley et al., 2017). Site 17JC is located just north of the Carnegie Ridge at 00°10.83' S, 85°52.00'W and 2846 m water depth (Figure 2-1, circle), and has "baseline" ^{230}Th-derived ^{232}Th fluxes that are similar to those observed at site 8JC (i.e., ~1.3 μg cm^{-2} kyr^{-1}). However, the variability of the ^{230}Th-derived ^{232}Th flux changes is

Figure 2-2
Ages for MIS stage boundaries and Terminations I and II from Lisiecki and Raymo, 2004 (See Methods, Supplementary Figure 2-3). Seven radiocarbon ages and uncertainties plotted in red at base of figure (See Methods). **a,** $\delta^{18}O$ record from *N. dutertrei* as %VSMOW (dark blue line). **b,** ^{230}Th-normalized ^{232}Th flux, a proxy for dust flux (green circles). Green solid line connecting data represents a three-point running mean. **c,** ^{230}Th-normalized xsBa flux, a proxy for export production (purple circles). Purple solid line connecting data represents a three-point running mean. **d,** Authigenic uranium, a proxy for bottom-water oxygenation (teal circles). Teal solid line connecting the data represents a three-point running mean.

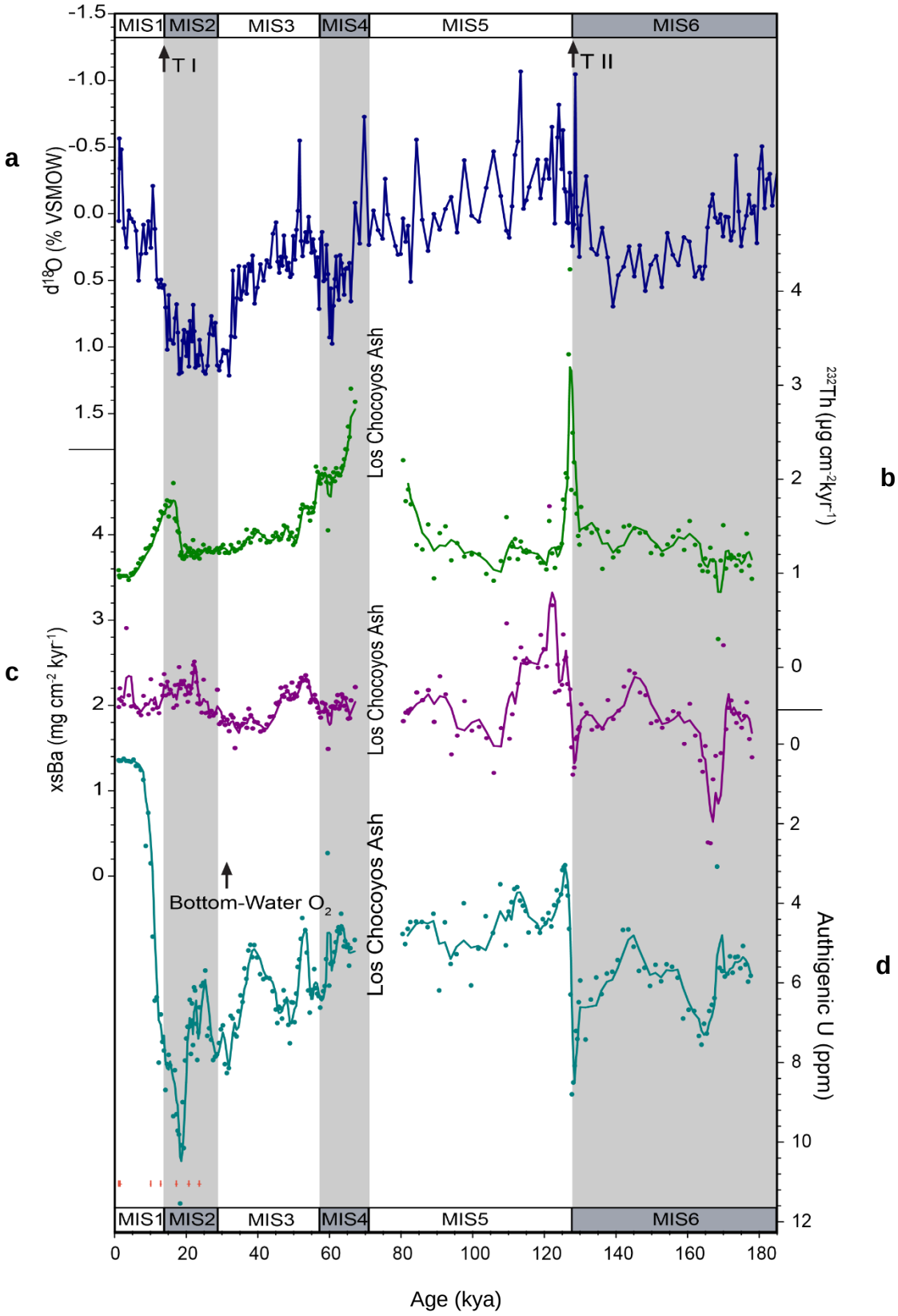
a
b
c
d
MIS1
MIS2
MIS3
MIS4
MIS5
MIS6
T I
T II
d18O (% VSMOW)
232Th (µg cm-2kyr-1)
Los Chocoyos Ash
xsBa (mg cm-2 kyr-1)
Bottom-Water O2
Authigenic U (ppm)
Age (kya)

greater at 17JC. Specifically, sediments from 17JC record significant ^{230}Th-derived ^{232}Th flux variability concurrent with the timing of several HS events (i.e., HS1, 2, 4, 5, 6, 7 and 9, Loveley et al., 2017). The disparity in ^{230}Th-derived ^{232}Th flux variability between our northern site (8JC) and the equatorial site (17JC) is likely related to the position of the ITCZ. At ~6° N, site 8JC, at a position that is close to that of the modern day ITCZ (~7° N; Donahoe et al., 2013), probably receives a supply of predominantly northern hemispheric dust. Therefore, the substantial increases in ^{230}Th-derived ^{232}Th flux recorded at site 8JC at the terminations and at the end of MIS 4 are simply the result of a dustier Northern Hemisphere at the end of glacial stages and are likely unrelated to shifts in the position of the ITCZ. On the other hand, Loveley et al. (2017), whose record spanned the last 90 kyr and did not reach the penultimate termination, hypothesized that ^{230}Th-derived ^{232}Th flux increases coincident with several HS events likely were associated with shifts in the ITCZ, such that the ITCZ was centered on or south of the equator during each HS event. Their reasoning was based on the similar ITCZ shifts hypothesized to explain records near or on the South American continent. Specifically, Cariaco Basin sediments (Peterson et al., 2000) record a drier climate during HS events when the ITCZ was displaced further south, while further south in Peru (Kanner et al., 2012) and Brazil (Wang et al., 2004), climate was wetter during HS events, again suggesting a significant southward displacement of the ITCZ. That the 8JC ^{230}Th-derived ^{232}Th flux record does not show the significant millennial variability (i.e., HS events) observed in the 17JC record is further support for the idea that millennial increases in ^{230}Th-derived ^{232}Th flux at 17JC can be explained, in part, by a southward shift in the position of the ITCZ. While the ^{230}Th-derived ^{232}Th flux record

at 8JC is almost entirely influenced only by the changing dustiness of the northern hemisphere atmosphere at the terminations and at the end of MIS 4, the ^{230}Th-derived ^{232}Th flux record at 17JC, is additionally influenced by millennial southward shifts in the ITCZ consistent with timing of northern hemisphere HS events.

2.2. The xsBa Productivity Proxy in the Eastern Equatorial Pacific

Barium enrichment in ocean sediments occurs at several locations that underlie productive surface waters in the modern ocean (Dymond et al., 1992). Since barite ($BaSO_4$) constitutes most biogenically-produced barium in the ocean, fluxes of barite in marine environments have been widely used as a proxy to reconstruct paleoproductivity (Dymond et al., 1992; Francois et al., 1995; Paytan et al., 1996; Paytan and Griffith, 2007; Griffith and Paytan., 2012; Liguori et al., 2016). Excess Ba (xsBa) concentrations, that portion of the total barium sedimentary signal that is produced authigenically (i.e., barite precipitation), can be estimated by subtracting the aluminosilicate Ba delivered from the continent from the total sedimentary Ba (e.g., Loveley et al., 2017, Francois et al., 1995; Schroeder et al., 1997; Jacquet et al., 2005; Stern et al., 2017). This paleoproductivity proxy is sensitive to changing pore water redox conditions, such that sulfate-reducing conditions can lead to the remineralization of previously deposited barite and subsequent release of barium into sediment pore waters (Torres et al., 1996; van Os et al.,1991; McManus et al., 1998).

At site 8JC in the EEP, the ^{230}Th-derived xsBa flux has an average value of ~2 μg cm^{-2} kyr^{-1} and a low variability (~1.2-2.8 μg cm^{-2} kyr^{-1}, Figure 2-2 B). Importantly, this site, which is north of the high productivity zone associated with the Pacific cold

tongue, has an average ^{230}Th-derived xsBa flux approximately half that of site 17JC (average of ~ 4 μg cm^{-2} kyr^{-1}), which is located in the upwelling zone to the south (Loveley et al., 2017). The position of core 17JC beneath the high-productivity waters of the equator is probably the cause of the disparity between the xsBa concentrations between at 8JC versus those at 17JC. Importantly, while there is a two-fold difference between average ^{230}Th-derived xsBa fluxes between sites 8JC and 17JC, there is not a similar disparity between the average aU concentrations recorded for the two cores. Indeed, excluding the Holocene part of the record the range in authigenic uranium (aU) values in both cores is from about 4 to 12 ppm. Authigenic uranium is also sensitive to sediment pore water redox conditions and its enrichment is a function of both the flux of reducible organic matter to the sediments (Anderson, 1982; Anderson et al., 1998; Chase et al., 2001; Francois et al., 1993; McManus et al., 2005) and the bottom water oxygen concentration of the overlying water (Zheng et al., 2002; Calvert and Pedersen, 1993; Francois et al., 1997). The disparity in average ^{230}Th-derived xsBa fluxes and lack of significant difference in average aU concentrations at both sites suggests that, in the case of 8JC and 17JC, sediment pore water redox conditions are primarily controlled by the oxygen content of bottom waters overlying the sediment, and not the sedimentary flux of organic matter. In addition, there is an anticorrelation (r=-0.536) between the flux of xsBa into the sediment and the concentration of preserved authigenic uranium in core 8JC from ~50-178 kyr (Figure 2-2). The anticorrelation of these two redox sensitive proxies suggest that, during the presence of hypoxic conditions in the sediment (higher aU), some amount of preserved, biogenically produced xsBa may have been remineralized and lost to the overlying bottom waters. This has been identified as a

significant limitation of the xsBa productivity proxy by McManus et al. (1998). Similarly, during periods of more oxic redox conditions (lower aU), xsBa preservation was likely increased. No similar anticorrelation between xsBa flux and aU concentration exists at site 17JC, indicating that at this site the xsBa concentration is controlled primarily by upwelling associate biologic productivity and that the xsBa record has not undergone significant alteration (Loveley et al., 2017), perhaps because of higher sedimentation rates. Indeed, Marcantonio et al. (2019) have shown during intense periods of hypoxia at site 17JC (aU values higher than 10 ppm), although low-O_2 waters probably dissolved barite (cf., 8JC), the dissolved xsBa did not completely escape the pore waters. Instead, at 17JC, the xsBa diffused downwards only slightly before reprecipitating a few cm lower in the record, in a more oxygenated interval of the sediment pile (Marcantonio et al., 2019). Ultimately, at site 8JC the low sedimentary fluxes of biogenically-produced barium and the anticorrelation between xsBa and aU from ~50-178 kya suggest that of sediment redox conditions were primarily driven by changes in bottom-water oxygen values rather than the flux organic matter into the sediment.

2.3. Deep Ocean Carbon Storage in the EEP

Currently, primary productivity in the EEP is both silica- and iron-limited (Moore et al., 2004), resulting in an inability for the carbon-sequestering abilities of the biological pump to compete with the CO_2 efflux generated from upwelling (Dugdale and Wilkerson, 1998). However, it has been shown that past relaxation of nutrient limitation in equatorial waters could have dampened this net CO_2 efflux (Loveley et al., 2017;

Martinez-Boti et al., 2015; Calvo et al., 2011; Pichevin et al., 2009) during the deglaciation. In the modern-day eastern Pacific Ocean (north of 12° S) waters deeper than 1 km (2 km north of the equator) are typically oxic ($[O_2] > 120$ µmol kg^{-1}), with hypoxic ($[O_2] < 60$-120 µmol kg^{-1}) and minor amounts of suboxic waters ($[O_2] < 2$-10 µmol kg^{-1}) occurring at shallower depths (Bianchi et al., 2012). Half of the respired organic carbon stored in the modern Pacific Ocean, the world's largest sink for respired carbon, is located in the upper 1.5 km (Bianchi et al., 2012). There is substantial evidence for a deepening of oxygen depleted waters in the EEP during the last glacial period (MIS 2) (de la Fuente et al., 2017; Doss and Marchitto, 2013; Hoogakker et al., 2018; Umling and Thunell, 2018; Robinson et al., 2009).

While the majority of ocean basins today have prevailing oxic to sub-oxic bottom water conditions, some hypoxic to anoxic basins do exist in areas where the organic matter exported to the sediments is oxidized faster than oxygen can be replenished. Within near-surface oceanic sediments, transitions from oxic to sub-oxic to anoxic conditions are driven by the oxidation of organic matter. This organic matter oxidation follows a well-constrained redox ladder as more thermodynamically favored oxidants are utilized at shallower depth intervals within the sediment (Froelich et al., 1978). Dissolved uranium present in pore waters exhibits similar redox behavior to iron. Near the sub-oxic-anoxic boundary in sediment, iron is reduced from Fe(III)-Fe(II) and uranium, present as the highly soluble $UO_2(CO_3)_3^{4-}$ complex, is reduced from U(VI) to U(IV), leading to the precipitation of authigenic uranium, presumably as insoluble uranium oxide (Barnes and Cochran, 1990). Authigenic uranium enrichment can, therefore, be produced by high rates of organic carbon deposition (Anderson, 1982;

Anderson et al., 1998; Chase et al., 2001; Francois et al., 1993; McManus et al., 2005), or changes in bottom water oxygenation values (Zheng et al., 2002; Calvert and Pedersen, 1993; Francois et al., 1997).

We have argued that authigenic uranium concentrations at 8JC are likely controlled by changing bottom-water oxygen levels rather than changes in organic carbon flux, and peak during glacial stages (MIS 2 and 6). At each of these stages, we hypothesize that the timing during which bottom-water oxygen concentrations (i.e., highest aU concentrations) are lowest is consistent with the timing during which the extent of a respired carbon pool was increased in the deep equatorial Pacific Ocean (i.e., lower bottom-water O_2 concentrations occur in tandem with high respired carbon storage), and when atmospheric CO_2 was low. The same interpretation was made based on aU results from nearby equatorial core, 17JC (Loveley et al., 2017). The two aU records, one from ~6° N at 1993 m water depth (8JC) and the other at the equator at 2846 m water depth (17JC), allow for a comparative reconstruction (Figure 2-3 B and C) over the past 95 kyr of past variations in EEP oceanic carbon storage at different bottom water depths.

Sediments in both EEP cores 17JC and 8JC indicate increasing trends in aU values from MIS 5 to MIS 2 (Figure 2-3 B and C). This pattern of aU at both sites (i.e., hypothesized decreasing bottom water O_2 values) is consistent with the idea that there is a gradual and coincident increase in storage of a respired carbon pool, as atmospheric CO_2 is lowered, over a significant swath of the EEP leading up to maximum storage (minimum in CO_2) during MIS 2. At 8JC, with the longer record encompassing the penultimate glacial period, the highest aU concentrations occur at glacial terminations II

and I. We suggest that these terminations mark a culmination of respired carbon storage in the EEP, which is consistent with the lowest observed global atmospheric CO_2 values over the past 140 kyr.

Importantly, there are several periods of disagreement between the 8JC and 17JC aU records. There are significant disparities between these EEP aU records during MIS 4 and late MIS 3-late MIS 2. This disparity in aU concentrations at the two sites seems to be greatest at times when the Antarctic ice core record shows pronounced and prolonged episodes of low CO_2 (180-200 ppm during MIS 2 and MIS 4). The difference between the aU in the two records could conceivably be explained if one considers the difference in depth between the two sites (8JC: 1993 m, 17JC: 2846 m). In the Pacific Ocean, respired carbon storage is thought to have increased at depths greater than 2 km during the last glacial maximum (LGM) (Jaccard et al., 2009; Jaccard et al., 2014; Herguera et al., 2010). At 2846 m water depth, core 17JC in the Panama Basin is well within the expected depth range associated with glacial increases in deep Pacific respired carbon storage. However, off-equatorial site 8JC is slightly above the 2 km depth estimate for deep waters which show an increased glacial respired carbon storage. This fact could result in the more variable nature of the 8JC aU record, as well as the aU enrichment disparities observed between it and the aU at 17JC. In this context, it is possible that the decreases in aU enrichment at site 8JC associated with rapid increases in aU enrichment at site 17JC result from changes in the depth and/or thickness of the respired carbon pool in the EEP. Importantly, decreases in aU values at site 8JC seem to happen much less rapidly than those at site 17JC, an observation which suggests that site

8JC is under the influence of oxygen-depleted waters for longer periods of time.

Moreover, the aU record for site 8JC at 1993 m depth, in comparison to that for site 17C

Figure 2-3
Ages for MIS stage boundaries and Terminations I and II from Lisiecki and Raymo, 2004. **a,** Authigenic U record from subarctic north Pacific Ocean core ODP 882 (red circles; Jaccard et al., 2009). Red line connecting the data represents a three-point running mean. **b,** Authigenic U record from EEP/Cocos ridge core MV1014-8JC (teal circles). Teal line connecting data represents a three-point running mean. **c,** Authigenic U record from EEP/Carnegie ridge core MV1014-17JC (gold circles). Gold line connecting data represents a three-point running mean. **d,** Authigenic U composite record from cores TN057-13PC (0-20 kya) and TN057-14PC (20-80 kya) from the Southern Ocean (red-brown; Jaccard et al., 2016). Red-brown line connecting the data represents a three-point running mean. **e,** Atmospheric CO_2 record from Antarctic ice cores (magenta circles; Bereiter et al., 2012)

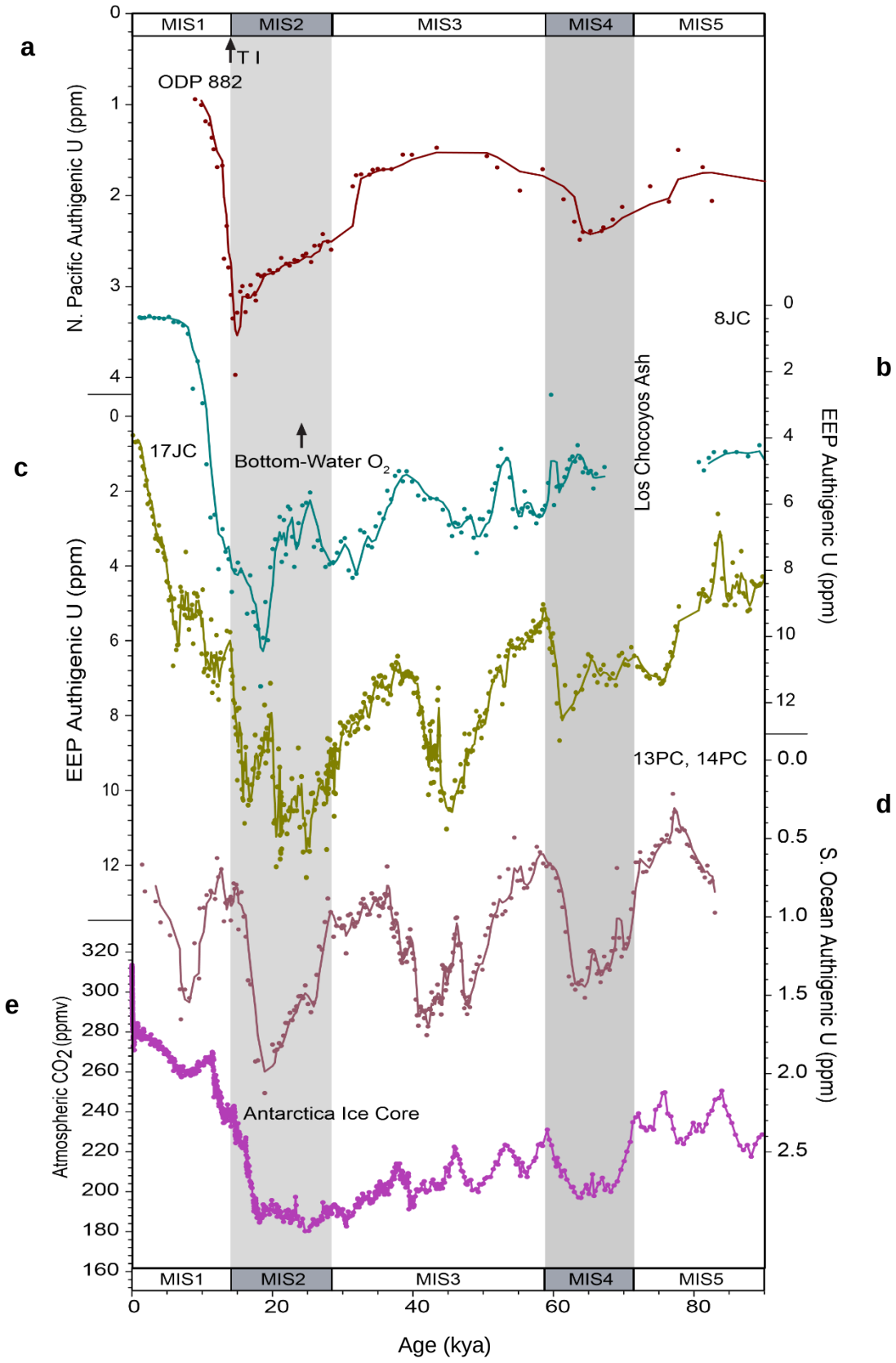
a
b
c
d
e
MIS1
MIS2
MIS3
MIS4
MIS5
T I
ODP 882
N. Pacific Authigenic U (ppm)
8JC
17JC
Bottom-Water O2
Los Chocoyos Ash
EEP Authigenic U (ppm)
13PC, 14PC
S. Ocean Authigenic U (ppm)
Atmospheric CO2 (ppmv)
Antarctica Ice Core
Age (kya)

at 2846 m, suggests that during times of minimum atmospheric CO_2 during the last glacial (MIS 2 and 4), storage of the respired carbon pool in the EEP deepens to depths of greater than 2 km.

2.4. Global Changes in Glacial-Interglacial Respired Carbon Storage and Atmospheric CO_2

Increased deep ocean respired carbon storage during the LGM has been demonstrated in the Southern (Jaccard et al., 2016; Martinez-Garcia et al., 2009) and Pacific Oceans (Jaccard et al., 2009; Anderson et al., 2008; Bradtmiller et al., 2010; Jaccard and Galbraith, 2011, Jacobel et al., 2017). Here, we compare aU high-resolution records from the Southern Ocean (TN057-13/14PC; Jaccard et al., 2016), the north subarctic Pacific (ODP Site 882; Jaccard et al., 2009) and the EEP (MV1014-17JC: Loveley et al., 2017; MV1014-8JC). We find that increases in authigenic uranium concentrations in each of these records occur at times during which there are decreases in bottom water oxygenation, which, in turn, are caused by increases in the storage of a respired carbon pool which, ultimately, is the driver of low glacial atmospheric CO_2 levels.

Records from cores 8JC and 17JC present a new case for multiple, repeated periods of deep ocean respired carbon storage in the EEP. These repeated storage events are strikingly similar to a record comprised of cores TN057-13PC (0-20 kya, 2800 m water depth) and TN057-14PC (20-80 kya, 3600 m water depth) from the Southern Ocean (Jaccard et al., 2016). Similar to EEP records from 8JC and17JC, this Southern Ocean composite record of aU enrichment demonstrates a general increasing linear trend

in concentrations from late stage MIS 5 to peak glaciation during MIS 2. This linear trend is suggestive of a gradual increase in respired carbon storage from ~85 kya up to the end of MIS 2, before relatively rapid oxygenation upon deglaciation. Moreover, all three records, particularly 17JC and 13/14PC demonstrate a synchronous, high aU variability at a period of ~20 kyr, highlighting the importance of both the Southern Ocean and the EEP in regards to long term oceanic storage of respired carbon (Figure 2-3 C and D). Authigenic uranium data from subarctic north Pacific site ODP 882 also demonstrates enhanced deep ocean respired carbon storage during Marine Isotope Stages 2 and 4. However, it does not show the higher-frequency variability observed in EEP cores 8JC/17JC and Southern Ocean cores 13/14PC, perhaps because much of the ODP 882 record beyond MIS 2 is of low resolution. However, a more complete comparison of the full aU records from cores 8JC and ODP 882 (Figure 2-4) demonstrates that since the penultimate glaciation (end MIS 6), deep ocean respired carbon storage has been gradually increasing in the EEP and subarctic north Pacific. It is important to note that peak aU enrichment at ODP 882 during MIS 6 occurs well before TII, at around 140 kyr. Moreover, the increase in aU concentrations at ODP 882 from MIS 6 to the LGM is half of that observed at site 8JC in the EEP. These differences, along with the fact that the subarctic north Pacific aU concentrations at ODP 882 are two to three times lower than those at EEP site 8JC, reinforce the relative importance of the EEP (along with the Southern Ocean) as being an important potential location for deep ocean respired carbon storage that are associated with periods of decreased global atmospheric CO_2 concentrations.

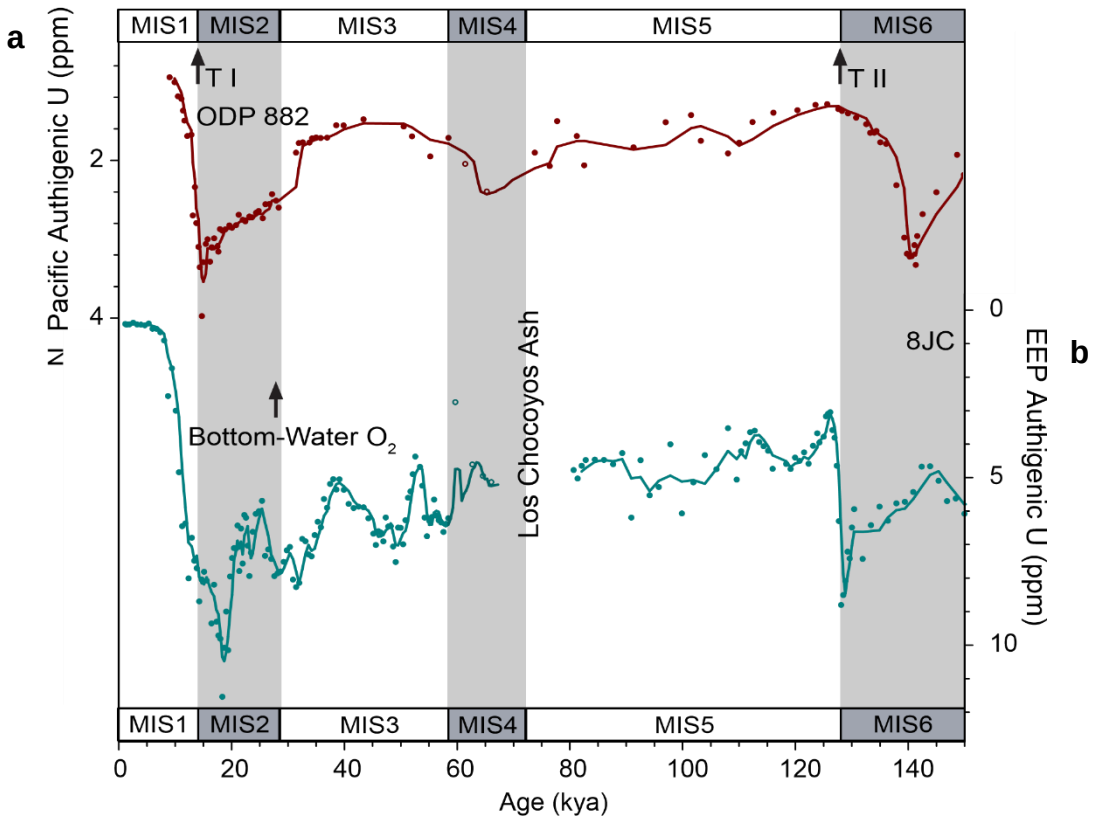

Figure 2-4
Ages for MIS stage boundaries and Terminations I and II from Lisiecki and Raymo, 2004 (See Methods, Supplementary Figure 2-3). **a,** Authigenic U record from subarctic north Pacific Ocean core ODP 882 (red circles; Jaccard et al., 2009). Red line connecting the data represents a three-point running mean. **b,** Authigenic U record from EEP/Cocos ridge core MV1014-8JC (teal circles). Teal line connecting data represents a three-point running mean.

3. METHODOLOGY

3.1. Analytical Methods.

Seven Radiocarbon analyses were performed on the first 100 cm of core MV1014-8JC on the planktonic foraminifer *Neogloboquadrina dutertrei* (>250 μm). Analyses were performed at the NOSAMS facility at the Woods Hole Oceanographic Institute. Radiocarbon ages were calibrated to calendar year using Calib 7.0 Marine13 (Stuiver and Reimer, 1993; Reimer et al., 2013) with a 400-yr reservoir age correction.

Oxygen isotope analyses were performed using a Thermo Electron Kiel IV sample preparation instrument with an attached Thermo MAT 253 stable isotope ratio mass spectrometer on samples of *N. dutertrei* specimens (>250 μm), and took place at the Stable Isotope Geoscience Facilities (SIGF) of Texas A&M University. Isotope values are reported in delta notation relative to the Vienna Standard Mean Ocean Water isotopic standard.

Sediments for MV1014-8JC were sampled approximately every 2 cm and analyzed for uranium (^{234}U, ^{235}U, ^{238}U), thorium (^{230}Th, ^{232}Th) and barium (^{135}Ba, ^{137}Ba) using inductively coupled plasma mass spectrometry (ICP-MS) on a magnetic sector Element XR at Texas A&M University. To prepare samples for analysis, 0.3–0.4 g of sediment was spiked with ^{229}Th and ^{236}U and then digested in a cocktail of HNO_3, $HClO_4$ and HF. Following complete sediment digestion, an aliquot was removed, diluted, and spiked with ^{235}Ba for separate analysis. Samples for U-Th

analysis were then further processed through Fe-oxyhydroxide coprecipitation and subsequent anion exchange chromatography in order to separate the Th and U. The National Institute of Standards and Technology Uranium 500 Standard (NIST U500) was used to correct for instrumental mass bias and was analyzed multiple times within each 12 analyses batch of Th and U. A similar mass bias was assumed to correct both the Th and U isotope ratios.

3.2. Age Models.

We constructed a preliminary age model using 1) seven radiocarbon dates on *N. dutertrei* between 0 and 100 cm depth in core, 2) the Los Chocoyos ash (84 kyr) (Rose et al., 1999) identified at 311 cm in the core, and 3) tying the 8JC $\delta^{18}O$ record (*N. dutertrei*) to the LRO4 global oxygen isotope record (Lisiecki and Raymo, 2004) via the software Analyseries (Paillard et al., 1996) With these three age constraints in place, a linear correlation (r= 0.705) resulted between the records. The stage boundaries between MIS 4 and 5, and MIS 5 and 6 were the most difficult to discern, given the millennial structure in the oxygen-isotope data. The age model for core MV1014-17JC was further refined from Loveley et al. (2017). Given the strong correlation between the ^{230}Th MAR and HS events in 17JC, the age model was refined by tuning the additional millennial scale ^{230}Th MAR cycles between HS events to the NGRIP ice core record from 30 kyr to 95 kyr.

3.3. ^{230}Th Normalization.

The ability to accurately determine past sedimentary fluxes is crucial to reliable paleoclimate reconstructions. ^{230}Th is a particle reactive isotope and has a comparatively short residence time relative to its parent isotope ^{234}U (10s of years to 200-400 ky) (Bacon and Anderson, 1982; Henderson, 2002). Scavenging of aqueous ^{230}Th by settling particles leads to its ultimate deposition in marine sediments. The assumption that ^{230}Th flux represents its production rate in the water column allows for the determination of sedimentary mass accumulation rates (MARs). Important to the ^{230}Th flux method is the fact that it allows for differentiation between the vertical flux form the overlying water column and the flux of sediments redistributed by bottom water currents. The latter flux can be discerned by calculating ^{230}Th-derived sediment focusing factors (Ψ) (Suman and Bacon, 1989). The utility of focusing factors lies in their ability to measure periods of focusing and winnowing in different oceanic sedimentary environments.

^{230}Th is preferentially scavenged by fine grain particles because they have a higher surface area to volume ratio (Thomson et al., 1993; Kretschmer et al., 2010). There may exist, therefore, a biasing effect on the measured activities of ^{230}Th in areas that have also been subjected to grain size biasing during redistribution processes. This would ultimately affect ^{230}Th derived MARs as well. In a study by Kretschmer et al. (2010) the potential biasing of ^{230}Th-normalized sediment fluxes at highly focused Atlantic sites was modeled with an aim to correct for syndepositional grain size biasing. It was determined that only sites with focusing factors outside values of 5.9 showed significant biasing of the ^{230}Th-derived MARs. Within the Panama Basin, previous studies show

that there is no more than a 30% biasing of ^{230}Th-normalized MARs when Ψ is less than about 4 (Singh et al., 2011; Marcantonio et al., 2014; Loveley et al., 2017b). Average focusing factors for the interval of sediment deposited within each oxygen-isotope stage (MIS 1 through 6) are consistently less than 4. The highest average focusing factor is 4.5 during MIS 2. Furthermore, xs^{230}Th-normalized accumulation rates of proxies that are contained predominantly in the fine-grained fraction of the sediment (such as the ^{232}Th, xsBa and authigenic U proxies used here) are not significantly sensitive to the ^{230}Th fractionation observed during sediment redistribution processes, which seems to affect coarse-grained component accumulation rates to a greater extent (Singh et al., 2011; Marcantonio et al., 2014). This is probably due to the ^{230}Th being most heavily concentrated in the fine-grained component of the sediment (Marcantonio et al., 2014). Accumulation rates for proxies that are virtually entirely contained within the fine-grained component of the sediment can be approximated by multiplying the concentration of the proxy with the ^{230}Th-derived MAR.

3.4. ^{232}Th Flux.

Windblown dust is primarily supplied to ocean sediments from continental material, which has an average ^{232}Th crustal concentration of ~11 ppm (Taylor and McLennan., 1985). The finer fraction of continental dust contains elevated concentrations of ^{232}Th (<4 μm, ~14 ppm), and is isolated during long distance travel in the atmosphere (McGee et al., 2016). Numerous studies in the past have used ^{232}Th

as a proxy for windblown dust in the equatorial Pacific Ocean (for example, Winckler et al., 2008; Kienast et al., 2013; Anderson et al., 2009; Singh et al., 2011; Marcantonio et al., 2014; Costa et al., 2016; Jacobel et al., 2016; Loveley et al., 2017a; 2017b). In this study ^{232}Th flux estimations are performed by normalization to ^{230}Th-derived sediment MARs.

3.5. xsBa Flux.

The association between biogenic "excess" Ba (xsBa) delivered to ocean sediment as the mineral barite (Griffith and Paytan, 2012), and organic matter permits the use of xsBa fluxes as a proxy for past primary productivity productivity (Dymond et al., 1992) on glacial–interglacial (Costa et al., 2016; Winckler et al., 2016; Loveley et al., 2017) timescales. To calculate the xsBa concentration in sediment samples, the detrital Ba component must be subtracted. This detrital, or lithogenic component is estimated by multiplying the detrital Th concentration by the average upper crustal Ba/Th ratio of 51.4 (Taylor and McLennan, 1985). Because barite is primarily found in the contained in the sediment fine-grained fraction of <5 μm (Griffith and Paytan, 2012) ^{230}Th-derived xsBa fluxes are likely not biased by sydepositional sediment redistribution (Marcantonio et al., 2014)

3.6. Authigenic U Concentrations.

Uranium is supplied to the sediments by the deposition of organic matter, sediment pore water redox conditions, and diffusion from higher concentrations in bottom waters to lower concentrations in pore waters (Anderson et al., 1982; Barnes

and Cochran, 1990; Zheng et al., 2002; Colley et al., 1984; Thomas et al., 1993). In oxic sedimentary pore waters, uranium primarily exists in the oxidation state of U(VI), which is the form of the soluble uranyl carbonate species. However, when pore water redox conditions are more reducing, U(IV) forms as a more insoluble solid uranium oxide. The two primary controls on uranium enrichment in marine sediments are the flux of organic carbon and bottom water oxygen concentrations.

4. CONCLUSIONS

This study has illuminated past changes in EEP atmospheric circulation and ocean chemistry by the comparison of a shallower core (8JC) 6º N of the equator, and a deeper core (17JC) at the equator. The ^{232}Th dust flux records differ between the sites, where at site 8JC peaks in dust flux occur at the end of glacials, dust flux at site 17JC also demonstrates millennial variability. In the context of the modern EEP position of the ITCZ at ~7º N, this result indicates that the millennial variability in dust flux at site 17JC is likely the result of HS event related southward shifts in the ITCZ of at least 7º. Authigenic uranium records between the two cores suggest a gradual increase in deep ocean respired carbon storage in the EEP over the past 95 kyr. The periods of disagreement between the aU records may be caused by their relative depths. During extended periods of low atmospheric CO_2, aU tends to be enriched at deeper (2846 m) site 17JC prior to enrichment at shallower (1993 m) site 8JC, consistent with a glacial increase in respired carbon storage occurring preferentially at depths >2km.

Comparison of global aU records highlights the importance of the deep ocean as a carbon reservoir over the past 95 kyr. Records from the Southern Ocean, the subarctic North Pacific, and eastern equatorial Pacific all indicate a gradual increase in respired carbon storage leading up to the LGM. The remarkable similarities between deep EEP and Southern Ocean aU records highlights the importance of both regions for storing oceanic respired carbon during periods of low atmospheric CO_2.

REFERENCES

ANDERSON, R. F. 1982. Concentration, vertical flux, and remineralization of particulate uranium in seawater. *Geochimica et Cosmochimica Acta,* 46**,** 1293-1299.

ANDERSON, R. F., ALI, S., BRADTMILLER, L. I., NIELSEN, S. H. H., FLEISHER, M. Q., ANDERSON, B. E. & BURCKLE, L. H. 2009. Wind-Driven Upwelling in the Southern Ocean and the Deglacial Rise in Atmospheric CO_2. *Science,* 323**,** 1443.

ANDERSON, R. F., FLEISHER, M. Q. & LAO, Y. 2006. Glacial–interglacial variability in the delivery of dust to the central equatorial Pacific Ocean. *Earth and Planetary Science Letters,* 242**,** 406-414.

ANDERSON, R. F., FLEISHER, M. Q., LAO, Y. & WINCKLER, G. 2008. Modern CaCO3 preservation in equatorial Pacific sediments in the context of late-Pleistocene glacial cycles. *Marine Chemistry,* 111**,** 30-46.

ANDERSON, R. F., KUMAR, N., MORTLOCK, R. A., FROELICH, P. N., KUBIK, P., DITTRICH-HANNEN, B. & SUTER, M. 1998. Late-Quaternary changes in productivity of the Southern Ocean. *Journal of Marine Systems,* 17**,** 497-514.

BACON, M. P. & ANDERSON, R. F. 1982. Distribution of thorium isotopes between dissolved and particulate forms in the deep sea. *Journal of Geophysical Research: Oceans,* 87**,** 2045-2056.

BARNES, C. E. & COCHRAN, J. K. 1990. Uranium removal in oceanic sediments and the oceanic U balance. *Earth and Planetary Science Letters,* 97**,** 94-101.

BEREITER, B., LÜTHI, D., SIEGRIST, M., SCHÜPBACH, S., STOCKER, T. F. & FISCHER, H. 2012. Mode change of millennial CO_2 variability during the last glacial cycle associated with a bipolar marine carbon seesaw. *Proceedings of the National Academy of Sciences,* 109**,** 9755.

BIANCHI, D., DUNNE, J. P., SARMIENTO, J. L. & GALBRAITH, E. D. 2012. Data-based estimates of suboxia, denitrification, and N_2O production in the ocean and their sensitivities to dissolved O_2. *Global Biogeochemical Cycles,* 26**,** n/a-n/a.

BRADTMILLER, L. I., ANDERSON, R. F., SACHS, J. P. & FLEISHER, M. Q. 2010. A deeper respired carbon pool in the glacial equatorial Pacific Ocean. *Earth and Planetary Science Letters,* 299**,** 417-425.

BROECKER, W. S. 1982. Ocean chemistry during glacial time. *Geochimica et Cosmochimica Acta,* 46**,** 1689-1705.

CALVERT, S. E. & PEDERSEN, T. F. 1993. Geochemistry of Recent oxic and anoxic marine sediments: Implications for the geological record. *Marine Geology,* 113**,** 67-88.

CALVO, E., PELEJERO, C., PENA, L. D., CACHO, I. & LOGAN, G. A. 2011. Eastern equatorial pacific productivity and related-CO_2 changes since the last glacial period. *Proc Natl Acad Sci U S A,* 108**,** 5537-41.

CHASE, Z., ANDERSON, R. F. & FLEISHER, M. Q. 2001. Evidence from authigenic uranium for increased productivity of the glacial subantarctic ocean. *Paleoceanography,* 16**,** 468-478.

COLLEY, S., THOMSON, J., WILSON, T. & HIGGS, N. J. G. E. C. A. 1984. Post-depositional migration of elements during diagenesis in brown clay and turbidite sequences in the North East Atlantic. 48**,** 1223-1235.

COSTA, K. M., MCMANUS, J. F., ANDERSON, R. F., REN, H., SIGMAN, D. M., WINCKLER, G., FLEISHER, M. Q., MARCANTONIO, F. & RAVELO, A. C. 2016. No iron fertilization in the equatorial Pacific Ocean during the last ice age. *Nature,* 529**,** 519-22.

DE LA FUENTE, M., CALVO, E., SKINNER, L., PELEJERO, C., EVANS, D., MÜLLER, W., POVEA, P. & CACHO, I. 2017. The Evolution of Deep Ocean Chemistry and Respired Carbon in the Eastern Equatorial Pacific Over the Last Deglaciation. *Paleoceanography,* 32**,** 1371-1385.

DONOHOE, A., MARSHALL, J., FERREIRA, D. & MCGEE, D. 2012. The Relationship between ITCZ Location and Cross-Equatorial Atmospheric Heat Transport: From the Seasonal Cycle to the Last Glacial Maximum. *Journal of Climate,* 26**,** 3597-3618.

DOSS, W. & MARCHITTO, T. M. 2013. Glacial deep ocean sequestration of CO_2 driven by the eastern equatorial Pacific biologic pump. *Earth and Planetary Science Letters,* 377-378**,** 43-54.

DUGDALE, R. C. & WILKERSON, F. P. 1998. Silicate regulation of new production in the equatorial Pacific upwelling. *Nature,* 391**,** 270.

DYMOND, J., SUESS, E. & LYLE, M. 1992. Barium in Deep-Sea Sediment: A Geochemical Proxy for Paleoproductivity. *Paleoceanography,* 7**,** 163-181.

FIELD, C. B., BEHRENFELD, M. J., RANDERSON, J. T. & FALKOWSKI, P. 1998. Primary Production of the Biosphere: Integrating Terrestrial and Oceanic Components. *Science,* 281**,** 237.

FRANCOIS, R., BACON, M. P., ALTABET, M. A. & LABEYRIE, L. D. 1993. Glacial/interglacial changes in sediment rain rate in the SW Indian Sector of subantarctic Waters as recorded by ^{230}Th, ^{231}Pa, U, and δ^{15}N. *Paleoceanography,* 8**,** 611-629.

FRANCOIS, R., HONJO, S., MANGANINI, S. J. & RAVIZZA, G. E. 1995. Biogenic barium fluxes to the deep sea: Implications for paleoproductivity reconstruction. *Global Biogeochemical Cycles,* 9**,** 289-303.

FRANOIS, R., ALTABET, M. A., YU, E.-F., SIGMAN, D. M., BACON, M. P., FRANK, M., BOHRMANN, G., BAREILLE, G. & LABEYRIE, L. D. 1997. Contribution of Southern Ocean surface-water stratification to low atmospheric CO2 concentrations during the last glacial period. *Nature,* 389**,** 929.

FROELICH, P. N., KLINKHAMMER, G. P., BENDER, M. L., LUEDTKE, N. A., HEATH, G. R., CULLEN, D., DAUPHIN, P., HAMMOND, D., HARTMAN, B. & MAYNARD, V. 1979. Early oxidation of organic matter in pelagic sediments of the eastern equatorial Atlantic: suboxic diagenesis. *Geochimica et Cosmochimica Acta,* 43**,** 1075-1090.

GRIFFITH, E. M. & PAYTAN, A. 2012. Barite in the ocean - occurrence, geochemistry and palaeoceanographic applications. *Sedimentology,* 59**,** 1817-1835.

HENDERSON, G. M. 2002. Seawater (234U/238U) during the last 800 thousand years. *Earth and Planetary Science Letters,* 199**,** 97-110.

HERGUERA, J. C., HERBERT, T., KASHGARIAN, M. & CHARLES, C. 2010. Intermediate and deep water mass distribution in the Pacific during the Last Glacial Maximum inferred from oxygen and carbon stable isotopes. *Quaternary Science Reviews,* 29**,** 1228-1245.

HOOGAKKER, B. A. A., LU, Z., UMLING, N., JONES, L., ZHOU, X., RICKABY, R. E. M., THUNELL, R., CARTAPANIS, O. & GALBRAITH, E. 2018. Glacial expansion of oxygen-depleted seawater in the eastern tropical Pacific. *Nature,* 562**,** 410-413.

JACCARD, S. L. & GALBRAITH, E. D. 2011. Large climate-driven changes of oceanic oxygen concentrations during the last deglaciation. *Nature Geoscience,* 5**,** 151.

JACCARD, S. L., GALBRAITH, E. D., FRÖLICHER, T. L. & GRUBER, N. 2014. Ocean (de)oxygenation across the last deglaciation: insights for the future. *Oceanography,* 27**,** 26-35.

JACCARD, S. L., GALBRAITH, E. D., MARTINEZ-GARCIA, A. & ANDERSON, R. F. 2016. Covariation of deep Southern Ocean oxygenation and atmospheric CO_2 through the last ice age. *Nature,* 530**,** 207-10.

JACCARD, S. L., GALBRAITH, E. D., SIGMAN, D. M., HAUG, G. H., FRANCOIS, R., PEDERSEN, T. F., DULSKI, P. & THIERSTEIN, H. R. 2009. Subarctic Pacific evidence for a glacial deepening of the oceanic respired carbon pool. *Earth and Planetary Science Letters,* 277**,** 156-165.

JACOBEL, A. W., MCMANUS, J. F., ANDERSON, R. F. & WINCKLER, G. 2016. Large deglacial shifts of the Pacific Intertropical Convergence Zone. *Nature Communications,* 7**,** 10449.

JACOBEL, A. W., MCMANUS, J. F., ANDERSON, R. F. & WINCKLER, G. 2017. Repeated storage of respired carbon in the equatorial Pacific Ocean over the last three glacial cycles. *Nat Commun,* 8**,** 1727.

JACQUET, S. H. M., DEHAIRS, F., CARDINAL, D., NAVEZ, J. & DELILLE, B. 2005. Barium distribution across the Southern Ocean frontal system in the Crozet–Kerguelen Basin. *Marine Chemistry,* 95**,** 149-162.

KANNER, L. C., BURNS, S. J., CHENG, H. & EDWARDS, R. L. 2012. High-Latitude Forcing of the South American Summer Monsoon During the Last Glacial. *Science,* 335**,** 570.

KIENAST, M., KIENAST, S. S., CALVERT, S. E., EGLINTON, T. I., MOLLENHAUER, G., FRANÇOIS, R. & MIX, A. C. 2006. Eastern Pacific cooling and Atlantic overturning circulation during the last deglaciation. *Nature,* 443**,** 846.

KRETSCHMER, S., GEIBERT, W., M. RUTGERS VAN DER LOEFF, M. & MOLLENHAUER, G. 2010. *Grain size effects on ^{230}Thxs inventories in opal-rich and carbonate-rich marine sediments*.

LAMY, F., GERSONDE, R., WINCKLER, G., ESPER, O., JAESCHKE, A., KUHN, G., ULLERMANN, J., MARTINEZ-GARCIA, A., LAMBERT, F. & KILIAN, R. 2014. Increased Dust Deposition in the Pacific Southern Ocean During Glacial Periods. *Science,* 343**,** 403.

LIGUORI, B. T., ALMEIDA, M. G. & REZENDE, C. E. 2016. Barium and its Importance as an Indicator of (Paleo)Productivity. *An Acad Bras Cienc,* 88**,** 2093-2103.

LISIECKI, L. E. & RAYMO, M. E. 2005. A Pliocene-Pleistocene stack of 57 globally distributed benthic $\delta^{18}O$ records. *Paleoceanography,* 20.

LOVELEY, M. R., MARCANTONIO, F., LYLE, M., IBRAHIM, R., HERTZBERG, J. E. & SCHMIDT, M. W. 2017. Sediment redistribution and grainsize effects on ^{230}Th-normalized mass accumulation rates and focusing factors in the Panama Basin. *Earth and Planetary Science Letters,* 480**,** 107-120.

LOVELEY, M. R., MARCANTONIO, F., WISLER, M. M., HERTZBERG, J. E., SCHMIDT, MATTHEW W. & LYLE, M. 2017. Millennial-scale iron fertilization of the eastern equatorial Pacific over the past 100,000 years. *Nature Geoscience,* 10**,** 760-764.

MARCANTONIO, F., LOVELEY, M. R., SCHMIDT, M. W. & HERTZBERG, J. E. 2019. Reply to: No evidence for equatorial Pacific dust fertilization. *Nature Geoscience,* 12**,** 156-156.

MARCANTONIO, F., LYLE, M. & IBRAHIM, R. 2014. Particle sorting during sediment redistribution processes and the effect on 230Th-normalized mass accumulation rates. *Geophysical Research Letters,* 41**,** 5547-5554.

MARTINEZ-BOTI, M. A., MARINO, G., FOSTER, G. L., ZIVERI, P., HENEHAN, M. J., RAE, J. W., MORTYN, P. G. & VANCE, D. 2015. Boron isotope evidence for oceanic carbon dioxide leakage during the last deglaciation. *Nature,* 518**,** 219-22.

MARTÍNEZ-GARCIA, A., ROSELL-MELÉ, A., GEIBERT, W., GERSONDE, R., MASQUÉ, P., GASPARI, V. & BARBANTE, C. 2009. Links between iron supply, marine productivity, sea surface temperature, and CO_2 over the last 1.1 Ma. *Paleoceanography,* 24.

MCGEE, D., WINCKLER, G., BORUNDA, A., SERNO, S., ANDERSON, R. F., RECASENS, C., BORY, A., GAIERO, D., JACCARD, S. L., KAPLAN, M., MCMANUS, J. F., REVEL, M. & SUN, Y. 2016. Tracking eolian dust with helium and thorium: Impacts of grain size and provenance. *Geochimica et Cosmochimica Acta,* 175**,** 47-67.

MCMANUS, J., BERELSON, W. M., KLINKHAMMER, G. P., HAMMOND, D. E. & HOLM, C. 2005. Authigenic uranium: Relationship to oxygen penetration depth and organic carbon rain. *Geochimica et Cosmochimica Acta,* 69**,** 95-108.

MCMANUS, J., BERELSON, W. M., KLINKHAMMER, G. P., JOHNSON, K. S., COALE, K. H., ANDERSON, R. F., KUMAR, N., BURDIGE, D. J., HAMMOND, D. E., BRUMSACK, H. J., MCCORKLE, D. C. & RUSHDI, A. 1998. Geochemistry of barium in marine sediments: implications for its use as a paleoproxy. *Geochimica et Cosmochimica Acta,* 62**,** 3453-3473.

MCMANUS, J. F., FRANCOIS, R., GHERARDI, J. M., KEIGWIN, L. D. & BROWN-LEGER, S. 2004. Collapse and rapid resumption of Atlantic meridional circulation linked to deglacial climate changes. *Nature,* 428**,** 834.

MEKIK, F. A., ANDERSON, R. F., LOUBERE, P., FRANÇOIS, R. & RICHAUD, M. 2012. The mystery of the missing deglacial carbonate preservation maximum. *Quaternary Science Reviews,* 39**,** 60-72.

MOORE, J. K., DONEY, S. C. & LINDSAY, K. 2004. Upper ocean ecosystem dynamics and iron cycling in a global three-dimensional model. *Global Biogeochemical Cycles,* 18.

SCHROEDER, J. O., MURRAY, R. W., LEINEN, M., PFLAUM, R. C. & JANECEK, T. R. 1997. Barium in equatorial Pacific carbonate sediment: Terrigenous, oxide, and biogenic associations. *Paleoceanography,* 12**,** 125-146.

PAILLARD, D., LABEYRIE, L. & YIOU, P. 1996. Macintosh Program performs time-series analysis. 77**,** 379-379.

PAYTAN, A. & GRIFFITH, E. M. 2007. Marine barite: Recorder of variations in ocean export productivity. *Deep Sea Research Part II: Topical Studies in Oceanography,* 54**,** 687-705.

PAYTAN, A., KASTNER, M. & CHAVEZ, F. P. 1996. Glacial to Interglacial Fluctuations in Productivity in the Equatorial Pacific as Indicated by Marine Barite. *Science,* 274**,** 1355.

PETERSON, L. C., HAUG, G. H., HUGHEN, K. A. & RÖHL, U. 2000. Rapid Changes in the Hydrologic Cycle of the Tropical Atlantic During the Last Glacial. *Science,* 290**,** 1947.

PICHEVIN, L. E., REYNOLDS, B. C., GANESHRAM, R. S., CACHO, I., PENA, L., KEEFE, K. & ELLAM, R. M. 2009. Enhanced carbon pump inferred from relaxation of nutrient limitation in the glacial ocean. *Nature,* 459**,** 1114-7.

REIMER, P. J., BARD, E., BAYLISS, A., BECK, J. W., BLACKWELL, P. G., RAMSEY, C. B., BUCK, C. E., CHENG, H., EDWARDS, R. L. & FRIEDRICH, M. J. R. 2013. IntCal13 and Marine13 radiocarbon age calibration curves 0–50,000 years cal BP. 55**,** 1869-1887.

ROBINSON, R. S., MARTINEZ, P., PENA, L. D. & CACHO, I. 2009. Nitrogen isotopic evidence for deglacial changes in nutrient supply in the eastern equatorial Pacific. *Paleoceanography,* 24.

ROSE, W. I., CONWAY, F. M., PULLINGER, C. R., DEINO, A. & MCINTOSH, W. C. 1999. An improved age framework for late Quaternary silicic eruptions in northern Central America. *Bulletin of Volcanology,* 61**,** 106-120.

SINGH, A. K., MARCANTONIO, F. & LYLE, M. 2011. Sediment focusing in the Panama Basin, Eastern Equatorial Pacific Ocean. *Earth and Planetary Science Letters,* 309**,** 33-44.

STERN, J., DELLWIG, O. & WANIEK, J. J. 2017. Deep–sea fluxes of barium and lithogenic trace elements in the subtropical northeast Atlantic. *Deep Sea Research Part I: Oceanographic Research Papers,* 122**,** 72-80.

STUIVER, M. & REIMER, P. J. 1993. Extended 14C Data Base and Revised CALIB 3.0 14C Age Calibration Program. *Radiocarbon,* 35**,** 215-230.

SUMAN, D. O. & BACON, M. P. 1989. Variations in Holocene sedimentation in the North American Basin determined from 230Th measurements. *Deep Sea Research Part A. Oceanographic Research Papers,* 36**,** 869-878.

TAKAHASHI, T., SUTHERLAND, S. C., WANNINKHOF, R., SWEENEY, C., FEELY, R. A., CHIPMAN, D. W., HALES, B., FRIEDERICH, G., CHAVEZ, F., SABINE, C., WATSON, A., BAKKER, D. C. E., SCHUSTER, U., METZL, N., YOSHIKAWA-INOUE, H., ISHII, M., MIDORIKAWA, T., NOJIRI, Y., KÖRTZINGER, A., STEINHOFF, T., HOPPEMA, M., OLAFSSON, J., ARNARSON, T. S., TILBROOK, B., JOHANNESSEN, T., OLSEN, A., BELLERBY, R., WONG, C. S., DELILLE, B., BATES, N. R. & DE BAAR, H. J. W. 2009. Climatological mean and decadal change in surface ocean pCO_2, and net sea–air CO_2 flux over the global oceans. *Deep Sea Research Part II: Topical Studies in Oceanography,* 56**,** 554-577.

TAYLOR, S. R. & MCLENNAN, S. M. 1985. The continental crust: Its composition and evolution. Blackwell Scientific, Oxford.

THOMSON, J., HIGGS, N. C., CROUDACE, I. W., COLLEY, S. & HYDES, D. J. 1993. Redox zonation of elements at an oxic/post-oxic boundary in deep-sea sediments. *Geochimica et Cosmochimica Acta,* 57**,** 579-595.

TOGGWEILER, J. R. 1999. Variation of atmospheric CO2 by ventilation of the ocean's deepest water. *Paleoceanography,* 14**,** 571-588.

TORRES, M. E., BRUMSACK, H. J., BOHRMANN, G. & EMEIS, K. C. 1996. Barite fronts in continental margin sediments: a new look at barium remobilization in the zone of sulfate reduction and formation of heavy barites in diagenetic fronts. *Chemical Geology,* 127**,** 125-139.

UMLING, N. E. & THUNELL, R. C. 2018. Mid-depth respired carbon storage and oxygenation of the eastern equatorial Pacific over the last 25,000 years. *Quaternary Science Reviews,* 189**,** 43-56.

VAN OS, B. J. H., MIDDELBURG, J. J. & DE LANGE, G. J. 1991. Possible diagenetic mobilization of barium in sapropelic sediment from the eastern Mediterranean. *Marine Geology,* 100**,** 125-136.

WANG, X., AULER, A. S., EDWARDS, R. L., CHENG, H., CRISTALLI, P. S., SMART, P. L., RICHARDS, D. A. & SHEN, C.-C. 2004. Wet periods in northeastern Brazil over the past 210 kyr linked to distant climate anomalies. *Nature,* 432**,** 740.

WINCKLER, G., ANDERSON, R. F., FLEISHER, M. Q., MCGEE, D. & MAHOWALD, N. 2008. Covariant Glacial-Interglacial Dust Fluxes in the Equatorial Pacific and Antarctica. *Science,* 320**,** 93.

ZHENG, Y., ANDERSON, R. F., VAN GEEN, A. & FLEISHER, M. Q. 2002. Remobilization of authigenic uranium in marine sediments by bioturbation. *Geochimica et Cosmochimica Acta,* 66**,** 1759-1772.

APPENDIX A

Average Depth (cm)	Age (kya)	δ18O (%VSMOW)	232Th Flux (ug/cm2/kyr)	aU (ppm)	xsBa flux (mg/cm2/kyr)
1	1.132	0.052	1.048	0.378	1.993
3	1.281	-0.567	0.992	0.395	2.085
5	1.430	-0.342	0.972	0.396	2.211
7	1.847	-0.484	0.986	0.391	2.064
9	2.532	0.105	0.987	0.341	2.024
11	3.217	0.251	0.987	0.395	2.916
13	3.902	-0.026	0.944	0.400	2.130
15	4.588	0.035	1.012	0.418	2.000
17	5.273	0.060	1.023	0.364	2.008
19	5.958	0.125	1.058	0.522	1.988
21	6.644	0.498	1.121	0.524	1.929
23	7.329	0.299	1.168	0.625	1.896
25	8.014	0.080	1.183	0.872	2.123
27	8.699	0.294	1.276	2.531	2.027
29	9.385	0.054	1.285	1.701	1.911
31	10.070	0.253	1.313	2.966	2.318
33	10.639	-0.211	1.418	4.807	1.968
35	11.207	0.111	1.494	6.414	2.036
37	11.776	0.492	1.475	6.328	1.985
39	12.344	0.548	1.582	7.970	1.922
41	12.913	0.491	1.670	6.761	2.254
43	13.350	0.552	1.648	7.448	2.126
45	13.786	0.531	1.653	7.667	2.378
47	14.223	0.699	1.738	8.657	2.127
49	14.659	1.015	1.788	8.006	2.289
51	15.096	0.606	1.617	7.774	2.147
53	15.532	0.941	1.776	8.037	2.193
57	16.405	0.971	1.970	9.314	1.983
59	16.842	0.779	1.594	8.160	2.249
61	17.278	0.676	1.567	9.265	2.013
63	17.623	0.886	1.461	9.678	2.256
65	17.968	1.197	1.446	9.773	2.460
67	18.313	1.084	1.205	11.505	2.210

69	18.658	1.186	1.241	10.041	2.259
71	19.003	0.948	1.172	8.962	2.266
73	19.348	0.867	1.168	10.113	2.299
75	19.693	0.965	1.310	7.916	2.134
77	20.038	1.063	1.193	7.363	2.226
79	20.383	0.885	1.282	7.069	2.054
81	20.728	1.142	1.242	7.082	2.245
83	21.025	0.800	1.281	6.394	2.150
85	21.323	0.940	1.202	7.751	2.213
87	21.620	0.954	1.231	6.486	2.391
89	21.918	0.680	1.368	7.529	2.486
91	22.215	0.877	1.179	6.080	2.525
93	22.512	1.150	1.192	6.161	2.401
95	22.810	1.112	1.226	6.998	2.284
97	23.107	1.056	1.192	7.903	2.036
99	23.405	1.133	1.259	7.206	2.132
101	23.702	0.942	1.170	6.583	2.024
103	24.251	1.055	1.246	6.046	1.929
105	24.799	1.177	1.318	5.967	2.313
107	25.348	1.196	1.267	5.657	1.923
109	25.896	1.136	1.242	7.299	1.929
111	26.445	0.897	1.283	7.107	1.880
113	26.993	0.764	1.239	7.394	1.950
115	27.542	0.907	1.236	7.905	1.892
117	28.090	0.814	1.260	7.822	1.922
119	28.639	1.133	1.281	7.762	2.195
121	29.187	1.170	1.232	7.478	1.795
123	29.736	1.103	1.289	7.134	1.817
125	30.284	1.016	1.318	7.035	1.874
127	30.833	1.042	1.232	8.009	1.784
129	31.381	1.025	1.234	8.232	1.846
131	31.930	1.209	1.230	8.108	1.712
133	32.478	0.914	1.317	6.795	1.901
135	33.027	0.422	1.280	6.862	1.870
137	33.576	0.922	1.247	7.259	1.514
139	34.124	0.628	1.260	7.312	1.798
141	34.673	0.389	1.342	6.679	1.761
143	35.221	0.640	1.280	6.283	1.777
145	35.770	0.576	1.311	6.447	1.798
147	36.318	0.393	1.347	5.604	1.854

149	36.867	0.596	1.479	5.865	1.751
151	37.415	0.373	1.382	5.154	1.972
153	37.964	0.428	1.340	5.011	1.897
155	38.512	0.310	1.442	5.321	1.743
157	39.061	0.671	1.476	5.017	1.820
159	39.837	0.550	1.462	5.331	1.815
161	40.711	0.375	1.368	5.750	1.707
163	41.585	0.499	1.408	5.874	1.722
165	42.459	0.345	1.340	5.830	1.790
167	43.334	0.396	1.346	5.853	1.879
169	44.208	0.147	1.411	6.178	1.883
171	45.082	0.062	1.446	6.637	2.038
173	45.521	0.356	1.405	6.976	2.022
175	45.959	0.440	1.369	6.566	2.053
177	46.397	0.319	1.378	6.607	2.217
179	46.835	0.386	1.430	6.865	2.127
181	47.272	0.160	1.523	6.155	2.113
183	47.710	0.323	1.508	6.423	2.231
185	48.148	0.418	1.504	6.414	2.179
187	48.586	0.364	1.374	7.022	2.087
189	49.024	0.472	1.409	7.485	2.082
191	49.462	0.451	1.446	6.455	2.278
193	49.900	0.163	1.316	6.465	2.094
195	50.338	0.342	1.343	6.955	2.132
197	50.776	0.117	1.407	6.236	2.117
199	51.214	-0.024	1.478	5.566	2.234
201	51.652	-0.551	1.617	5.379	2.273
203	52.070	0.202	1.698	4.861	2.336
205	52.488	0.315	1.744	4.338	2.300
209	53.323	0.135	1.716	4.642	2.365
211	53.741	0.210	1.716	5.207	2.300
213	54.159	0.021	1.652	6.158	2.226
215	54.576	0.133	1.573	6.715	2.047
217	54.994	0.290	1.711	6.254	2.079
219	55.412	0.188	1.663	6.143	2.080
221	55.830	0.278	1.761	5.621	2.135
223	56.247	0.469	2.145	6.102	2.054
225	56.665	0.324	2.090	6.241	1.983
227	57.083	0.710	2.002	6.303	1.927
229	57.501	0.185	1.964	6.588	1.870

231	57.918	0.134	2.065	6.347	2.046
233	58.336	0.502	2.053	6.177	1.939
235	58.754	0.489	2.123	6.051	2.027
237	59.172	0.231	1.983	5.369	1.946
239	59.589	0.450	1.470	2.710	1.504
241	60.006	0.923	2.046	6.038	1.908
243	60.378	0.556	1.967	5.487	1.996
245	60.751	0.971	2.018	5.439	2.002
247	61.123	0.687	2.085	5.442	1.999
249	61.496	0.487	1.991	5.193	1.979
251	61.868	0.317	2.130	4.948	2.055
253	62.241	0.544	2.076	4.666	2.133
255	62.613	0.642	2.054	4.571	1.973
257	62.986	0.307	2.051	4.724	2.007
259	63.358	0.367	2.131	4.233	2.142
261	63.731	0.454	2.153	4.621	2.107
263	64.103	0.604	2.223	5.048	2.007
265	64.476	0.411	2.330	4.914	2.096
267	64.848	0.403	2.325	5.072	1.959
269	65.221	0.407	2.570	5.003	1.857
271	65.593	0.366	2.459	5.535	1.863
273	65.966	0.653	2.971	5.098	2.071
275	67.168	-0.085	2.833	4.890	2.226
277	68.451	0.221	3.791	4.265	2.265
279	69.733	-0.728	3.677	4.441	2.175
281	71.015	0.231	4.999	4.200	2.172
283	72.298	-0.026	5.512	3.945	2.024
285	73.580	0.120	11.516	3.061	2.468
287	74.843	0.184	13.485	2.864	2.477
289	75.558	-0.264	26.302	2.142	2.524
291	76.273	0.004	27.866	2.097	2.586
293	78.419	0.239	130.043	1.516	5.555
295	79.134	0.304	106.873	1.587	4.061
297	79.849	0.299	18.309	2.587	2.109
299	80.564	0.033	2.213	4.740	1.828
301	81.279	0.208	1.779	4.992	1.928
303	81.994	0.087	1.903	4.612	1.953
305	82.709	0.507	1.746	4.440	1.972
307	84.324	-0.558	1.316	4.428	2.163
309	85.943	0.043	1.267	4.437	2.074

311	87.561	0.276	1.532	4.567	2.191
313	89.180	-0.001	0.961	4.233	1.820
315	90.798	0.116	1.440	6.159	2.352
317	92.417	-0.037	1.513	4.447	2.142
319	94.036	-0.129	1.153	5.493	1.440
321	95.654	0.138	1.335	5.248	1.659
323	97.693	-0.403	1.192	3.969	2.062
325	99.736	0.013	1.214	6.032	1.717
327	101.778	0.057	1.216	5.110	1.761
329	103.821	-0.197	1.009	4.294	1.630
331	105.864	-0.469	0.936	4.715	1.224
333	107.906	-0.136	1.146	3.491	1.747
335	109.450	0.124	1.610	5.024	2.970
337	110.246	0.176	1.173	4.176	1.623
339	111.042	-0.059	1.298	3.941	1.908
341	111.837	-0.443	1.379	3.610	2.565
343	112.633	-0.545	1.164	3.564	2.268
345	113.429	-1.068	1.353	3.903	2.691
347	114.225	-0.039	1.244	4.029	2.536
349	115.021	-0.104	1.235	4.163	2.503
351	115.817	-0.202	1.244	4.703	2.521
353	118.205	-0.408	1.181	4.555	2.453
355	119.001	-0.118	1.126	4.708	2.836
361	119.797	-0.262	1.127	4.368	2.672
363	120.593	-0.408	1.056	4.466	2.469
365	121.389	-0.265	1.569	4.212	4.340
367	122.184	-0.653	1.227	4.551	3.182
369	122.980	0.071	1.072	4.016	2.165
371	123.731	-0.575	1.281	3.642	2.491
373	124.114	-0.819	1.288	3.918	2.186
375	124.880	-0.337	1.328	3.744	2.253
377	125.263	-0.629	1.796	3.136	2.841
379	125.646	-0.189	1.699	3.060	2.543
381	126.029	-0.167	2.075	3.013	2.574
383	126.412	0.061	2.027	3.546	2.262
385	126.795	0.067	3.335	3.775	2.022
387	127.178	-0.310	4.236	4.612	2.200
389	127.561	-0.143	1.899	6.261	1.523
391	127.944	0.240	2.503	8.765	1.204
393	128.327	0.079	2.191	8.468	1.286

395	128.710	-1.047	1.858	8.047	1.620
397	129.093	-0.054	1.647	7.176	1.644
399	129.476	0.109	1.411	7.377	1.733
401	129.859	0.320	1.318	6.453	1.762
403	130.261	0.009	1.718	5.906	2.027
405	131.756	-0.284	1.491	7.390	1.929
407	133.251	0.259	1.445	6.386	1.727
409	134.746	0.304	1.480	5.831	1.763
411	136.241	0.102	1.062	6.250	1.742
413	137.737	0.324	1.456	5.732	2.074
415	139.232	0.692	1.183	5.688	1.851
417	140.727	0.458	1.247	5.393	1.950
419	142.222	0.394	1.508	4.638	2.231
421	143.717	0.243	1.523	4.626	2.421
423	145.212	0.467	1.493	5.059	2.388
425	146.709	0.234	1.442	5.665	2.162
427	148.252	0.575	1.448	5.589	2.131
429	149.795	0.380	1.229	6.044	1.803
431	151.339	0.313	1.301	5.513	1.830
433	152.882	0.547	1.212	5.928	1.751
435	154.425	0.141	1.321	5.499	1.851
437	155.968	0.305	1.405	5.562	1.944
439	157.511	0.382	1.470	5.838	1.922
441	159.054	0.173	1.263	6.864	1.564
443	160.598	0.206	1.569	6.645	2.031
445	162.141	0.470	1.317	6.672	1.660
447	163.474	0.394	1.101	7.300	1.368
449	164.199	0.485	1.040	7.518	1.237
451	164.924	0.391	1.171	6.994	1.538
453	165.649	0.100	1.034	7.240	0.413
455	166.374	-0.060	1.286	6.674	0.403
457	167.100	-0.149	1.154	6.518	1.149
459	167.825	0.026	0.983	6.350	1.423
461	168.550	0.065	0.319	3.049	0.026
463	169.275	0.002	1.150	5.590	1.455
465	170.000	0.167	1.524	5.672	2.716
467	170.725	0.019	1.066	5.809	1.734
469	171.450	0.023	1.178	5.738	1.983
471	172.176	0.198	1.208	5.301	2.070
473	172.901	0.130	1.183	5.711	1.912

475	173.626	-0.440	1.097	5.323	1.809
477	174.351	-0.019	1.209	5.309	1.921
479	175.076	0.241	1.041	5.600	1.752
481	175.801	0.108	1.195	5.041	1.890
483	176.526	0.013	1.435	5.509	2.048
485	177.252	-0.145	1.096	5.938	1.619
487	177.977	-0.005	0.956	5.787	1.406